Effects of Detuning on Wide-Temperature Behavior of 25 Gbaud 850 nm VCSELs

Effects of Detuning on Wide-Temperature Behavior of 25 Gbaud 850 nm VCSELs

Hans Daniel Kaimre[a], Alexander Grabowski[a], Johan Gustavsson[a], and Anders Larsson[a]

[a]Photonics Laboratory, Department of Microtechnology and Nanoscience, Chalmers University of Technology, SE-41296 Gothenburg, Sweden

ABSTRACT

Emerging markets for optical interconnects with VCSEL-based transceivers require VCSELs with superior wide temperature performance. One of the prime parameters controlling the temperature dependence of VCSEL performance is wavelength detuning. We study the impact of detuning on the performance of 25 Gbaud class 850 nm VCSELs over a temperature range of -40 to 125°C, as applicable to e.g. automotive optical networking. Two VCSELs with different detuning, but otherwise identical, are compared. Basic static and dynamic performance parameters and their temperature dependencies are extracted. The results show that with appropriate detuning, sufficient performance at the temperature extremes and improved tolerance to temperature variations can be achieved. Excessive detuning to meet the more challenging high temperature performance requirements leads to insufficient low temperature performance.

Keywords: Vertical-cavity surface-emitting laser, dynamics, temperature dependence, detuning.

1. INTRODUCTION

The vertical-cavity surface-emitting laser (VCSEL) is the light source of choice for short and very short reach optical interconnects (OIs). It can be directly modulated at high speed and enables the smallest footprint transceiver modules and the most energy and cost efficient interconnects.[1] Since energy and cost efficiency implies uncooled operation, it is the component of the optical channel that to the largest extent dictates the variation in channel response as the temperature changes.

While consumer applications currently retain the greatest VCSEL market share, largely stimulated by Apple's decision to use them in facial recognition technology in their smartphones, datacom has historically been the most prominent application of VCSELs. In addition, Yole's annual market study estimates that datacom could regain its supremacy and dominate the VCSEL market for the following five years, starting in 2023.[2] Currently, major providers of datacom VCSELs guarantee performance over a temperature range of 0 to 90 °C or less, depending on data rate and manufacturer.[3,4] New markets require VCSELs with a wider operating temperature range.

There are at least three markets that need VCSELs with superior wide- and high-temperature performance: high performance computing, automotive industry, and defense/military applications. In high performance computing systems, whether being a full-scale datacenter or a single high performance signal processing unit, electrical interconnects have been and are being replaced by OIs that allow for higher interconnect speed and higher energy efficiency. With increasing data rates, the electrical interconnects transporting data from the integrated circuits (ICs) on the circuit boards to the optical transceivers on the front panel cannot provide the bandwidth needed and the optical transceiver port count and density becomes excessive. Therefore, the transceivers have to migrate into the units, close to the ICs where temperature variations can be extreme and peak temperatures can reach up to 100 °C because of the close proximity to heat generating ICs.[5] Tough conditions are similarly expected in automotive applications. With the emergence of various sensors (radar, cameras, LIDAR and others) used for advanced driver-assistance systems, the amount of data transmitted inside the vehicle is ever-increasing and OIs pose a solution to these increased data rates. However, this environment

Further author information: (Send correspondence to Hans Daniel Kaimre)
Hans Daniel Kaimre: E-mail: kaimre@chalmers.se, Telephone: +46793596594

is even harsher, with temperatures ranging from −40 °C to 125 °C. Similar conditions are experienced for use in defense and military applications. VCSELs used in these applications must therefore have a superior wide-temperature performance.

The performance of VCSELs depends on ambient temperature through various mechanisms, the most fundamental being the reduction of gain and differential gain with increasing temperature. Simulations show that the material gain is reduced and the gain peak shifts towards longer wavelength at a considerable rate with increasing temperature, mostly due to the temperature dependence of the occupation probabilities (Fermi-distribution) in conduction and valence bands[6] and the reduction of the bandgap with increasing temperature in the quantum wells (QWs) in the active region of the VCSEL. Due to this, differential gain, which is an approximate measure of the operating speed of the VCSEL, shifts and decreases similarly.[6] These phenomena are inherent and have to be compensated for in the design of the device.

One of the parameters that has large impact on the temperature dependence of VCSEL performance is detuning, here defined as the wavelength difference between cavity resonance and active region photoluminescence (PL) peak at room temperature (RT). There is a ∼10 nm offset between PL and gain peak wavelengths, with the gain peak being at longer wavelength, but they shift at the same rate with temperature.[7] PL and gain peaks, as well as resonance wavelength, red-shift with increasing temperature. While the PL and gain peaks shift at a rate of 0.32 - 0.33 nm/K for an 850 nm VCSEL,[8] the resonance wavelength, determined by the cavity length, shifts at approximately 0.06 nm/K for the VCSELs used in this study. In Figure 1, the shifts of resonance wavelength, PL spectrum, and gain spectrum with temperature are illustrated. It can be seen that the modal gain changes with temperature due to the changing overlap of the resonance wavelength with the gain spectrum, which itself changes with temperature. Detuning has strong impact on the temperature dependence of VCSEL performance, most explicitly on the temperature dependence of threshold current, but it also affects other key performance parameters.

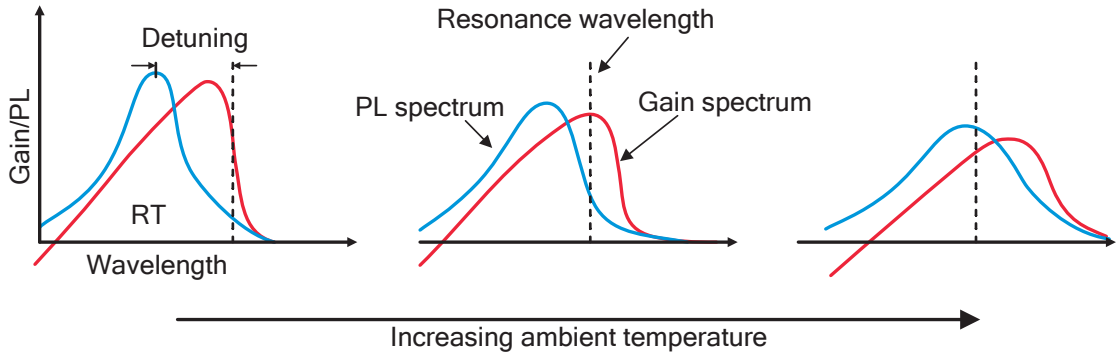

Figure 1: Schematic illustrating how PL and gain spectra and resonance wavelength shift with temperature. Gain and PL spectra are not to scale.

To compensate for the reduction of gain and differential gain with increasing temperature, one can choose an appropriate detuning. Differential gain is reduced with increasing carrier density and therefore depends on threshold current which sets the carrier density due to clamping. It is also important to note that differential gain drops less rapidly on the short wavelength side of the gain peak than on the long wavelength side, which has a substantial impact on the modulation dynamics of the VCSEL and its temperature dependence. By detuning the design accordingly, differential gain can be increased in a desired temperature range where the resonance wavelength is close to the gain peak. Since meeting performance requirements is most challenging at high temperatures, it is tempting to increase detuning to shift the threshold current minimum to a higher temperature, thereby improving the high temperature performance through lower carrier density and higher differential gain. This may, however, degrade performance at low temperatures.

To investigate the effects of detuning on the wide-temperature behavior of VCSELs, we have studied two 850

nm VCSEL designs with different detuning but otherwise identical. One has detuning set for minimum threshold current at around 0 °C. which is common for conventional datacom VCSELs (this way the laser operates on the short wavelength side of the gain peak over the limited temperature range). The other has larger detuning for minimum threshold current at around 70 °C and improved high temperature performance. DC, spectral and dynamic characteristics are measured over a wide range of temperatures (−40 to 125 °C) and currents and key performance parameters and their temperature dependencies are extracted.

2. HIGH-SPEED VCSEL DESIGNS

Two different epitaxial designs were used to fabricate the oxide-confined VCSELs used in this study. They are based on a previous design with 2 + 4 oxide layers for reduced capacitance and strained InGaAs/AlGaAs QWs for high differential gain, described in detail in Reference 9.

Different detuning is achieved by a small difference in In-content in the QWs. In the high-temperature design (A), the active region PL peak is at 830 nm at RT, while for the more conventional design (B) the PL peak is at 844 nm at RT. With both designs having a resonance wavelength of 850 nm at RT, the detuning is 20 nm (A) and 6 nm (B), respectively. The epitaxial structures were grown on n-type GaAs substrates. A thick layer of BCB was used to reduce pad capacitance. Both designs have identical resonator and distributed Bragg reflector (DBR) designs.

3. STATIC PERFORMANCE CHARACTERISTICS

In this section, we present the current-power-voltage (IPV) characteristics at different temperatures. To acquire the data, we used an MPI TS200-SE probe station that allows for measurements from −60 °C to 300 °C in a light-tight and moisture-free shielded test environment. The VCSELs were biased using a DC power source and light was collected with a large area photodetector for IP-measurements and with a lensed fiber (which outputs into an optical spectrum analyzer) for spectral measurements.

All the measurements were performed from −40 °C to 125 °C with 20-degree increments up to 120 °C. Some of the parameters are presented at limited temperatures for ease of understanding, other parameters that depend on both temperature and bias current are presented at 6, 7, 8 and/or 9 mA as these biases correspond to the typical current densities (20 to 30 kA/cm^2) occurring in the operation of datacom VCSELs.

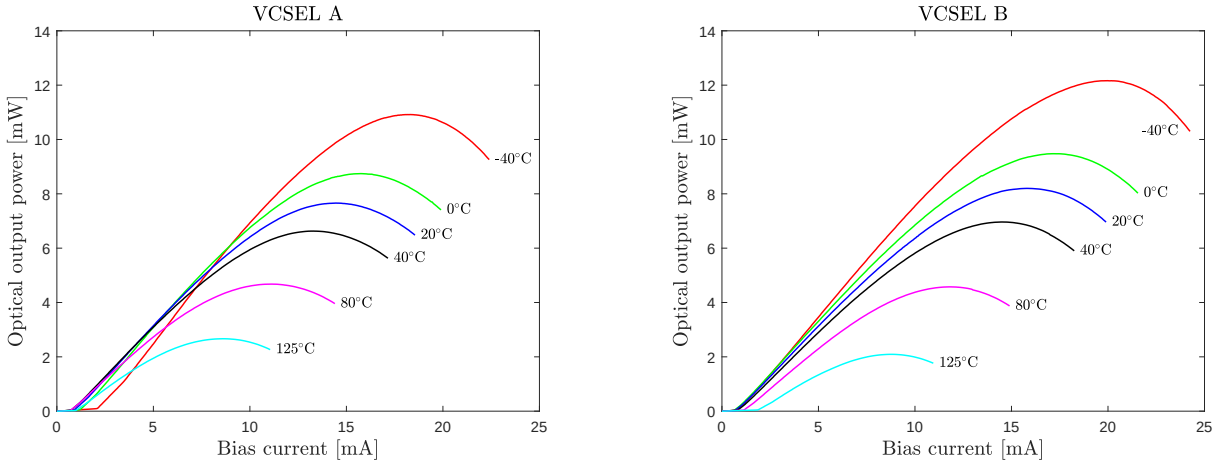

Figure 2: IP-characteristics for the two VCSELs at different ambient temperatures.

Figures 2 and 3 show IPV-characteristics at various ambient temperatures. Both VCSELs reach a maximum power of approximately 12 mW at −40 °C and the maximum power, along with the rollover current, decreases linearly with temperature and reaches approximately 2 mW at 125 °C. This very similar behavior is to be

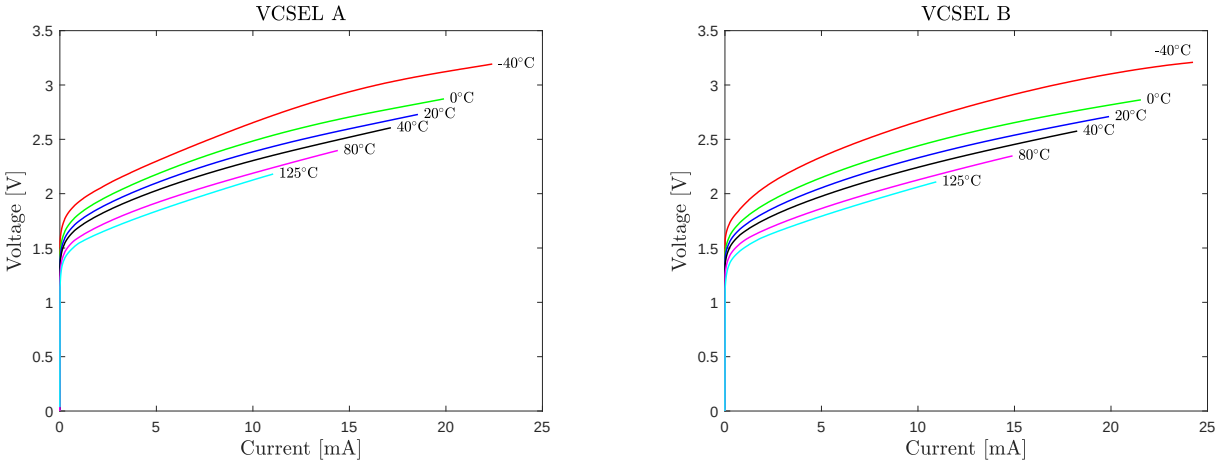

Figure 3: IV-characteristics for the two VCSELs at different ambient temperatures.

expected because of identical optical resonator and DBR configurations for the two VCSEL designs. From the IP-dependence (Figure 2) we can extract threshold currents and slope efficiencies. Differential resistance may be derived from the IV-characteristics (Figure 3). Differential resistance at 7 mA (displayed in Figure 4) is very similar for the two VCSELs, which is to be expected as the two designs have identical DBRs.

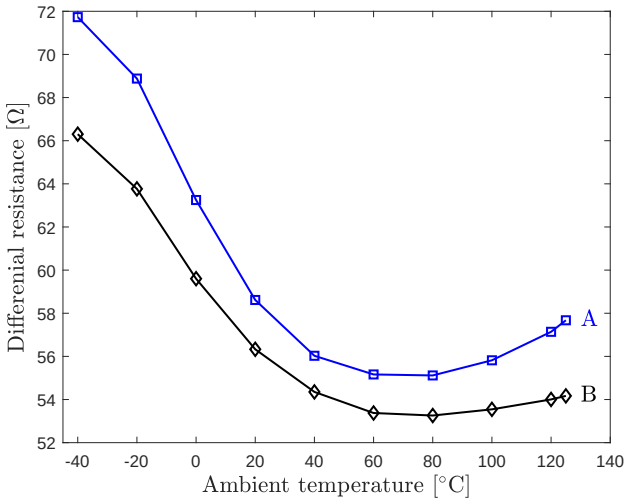

Figure 4: Differential resistance at 7 mA for VCSEL A and VCSEL B.

The difference in detuning between the two VCSELs translates to a large difference in the temperature dependence of the threshold current. Figure 5 shows that design A (detuning 20 nm) exhibits minimum threshold current at approximately 70 °C, while for design B (detuning 6 nm) minimum threshold current occurs at approximately 0 °C, which is typical for most present days datacom VCSELs. The minimum threshold current is nearly the same for the two designs. The greater variation for VCSEL A stems from the fact that at low temperatures the resonance wavelength coincides with the long-wavelength side of the gain spectrum where gain is more strongly dependent on wavelength (see Figure 1 for illustration).

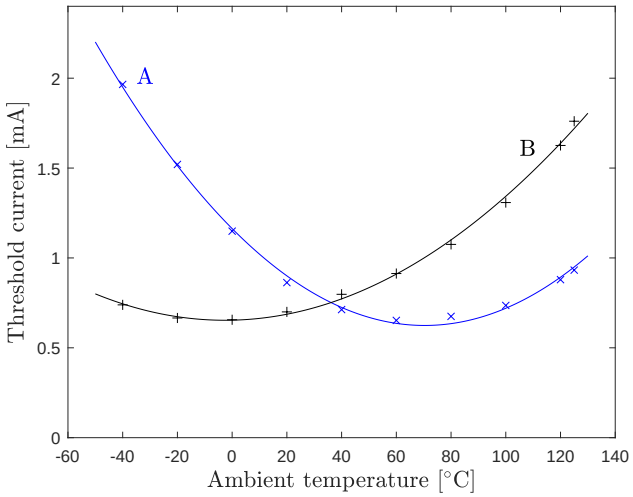

Figure 5: Dependence of threshold current on ambient temperature for the two VCSELs. Data points (+ and ×) indicate experimental data, while solid line shows a 2nd order polynomial fit.

Slope efficiency (SE) is determined from measured IP-curves and can, together with simulations accounting for the temperature dependence of optical loss rates, be used to estimate the temperature dependence of the internal quantum efficiency. SE at low currents, where current-induced self-heating has minor impact, can be approximated as

$$SE(T) = \frac{hc}{q\lambda(T)} \cdot \eta_{\mathrm{i}}(T) \cdot \frac{\alpha_{\mathrm{T}}(T)}{\alpha_{\mathrm{T}}(T) + \alpha_{\mathrm{B}}(T) + \alpha_{\mathrm{FCA}}(T)}, \tag{1}$$

where h is Planck's constant, c speed of light, q elementary charge, $\lambda(T)$ emission wavelength, $\eta_{\mathrm{i}}(T)$ internal quantum efficiency, $\alpha_{\mathrm{FCA}}(T)$ free carrier absorption loss rate, and $\alpha_{\mathrm{T}}(T)$ and $\alpha_{\mathrm{B}}(T)$ the transmission loss rates through the top and bottom DBRs, respectively. In Figure 6a, the SE at different temperatures is presented. There is a small difference between the two designs: VCSEL A exhibits a somewhat higher SE throughout the entire temperature range and for VCSEL B it decreases at a faster rate at high temperatures. This is caused by the higher threshold current at high temperatures, which translates to a higher carrier density and therefore enhanced thermally assisted carrier leakage. In addition to experimental results, results from simulations are presented in Figure 6a. These are obtained using equation 1 where temperature-dependent coefficients are used for all parameters except the internal quantum efficiency, which is set to $\eta_{\mathrm{i}} = 1$. Thus, dividing measured SE with the simulated, we obtain an estimate for the temperature dependence of internal quantum efficiency $\eta_{\mathrm{i}}(T)$ presented in Figure 6b. VCSEL A reaches a maximum internal quantum efficiency of 0.88 at 80 °C, while VCSEL B reaches a maximum internal quantum efficiency of 0.79 at 40 °C. The temperature dependence of η_{i} is correlated with the temperature dependence of threshold current: an increase in threshold current results in a higher carrier density which translates to more vertical leakage, driven by carrier density and temperature (thermionic emission).

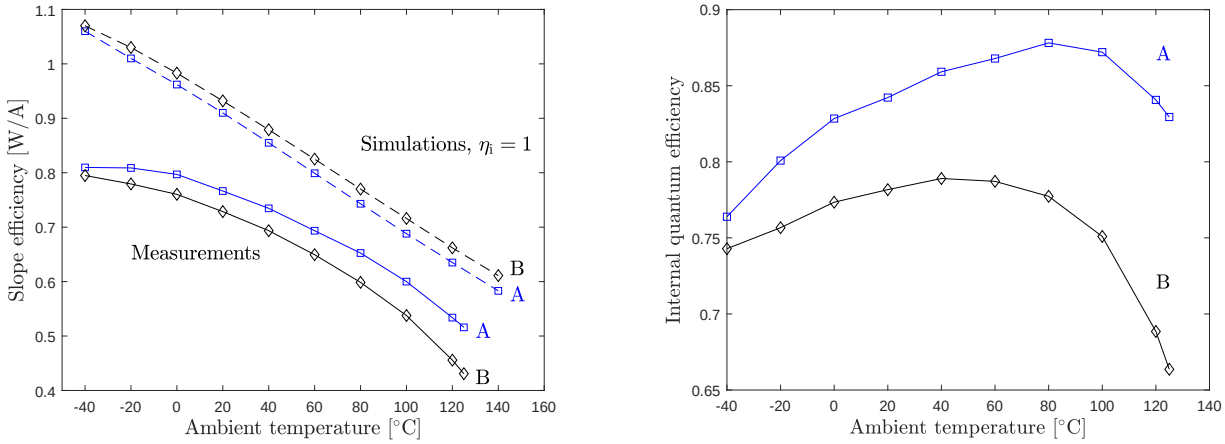

(a) (b)

Figure 6: a) Measured SE as a function of temperature together with calculated SE assuming unity internal quantum efficiency. b) Temperature dependence of internal quantum efficiency estimated from measured and calculated SE.

In addition to measuring the IPV-characteristics, we also measured spectra at different currents in the entire temperature range. Raw spectra are not presented here, but the VCSELs show multimode operation throughout the entire current and temperature range. The spectral measurements can be combined with IPV-measurements to deduce the thermal characteristics of the VCSELs. We used the method proposed by Daubenschüz and Michalzik[10] to determine the internal temperature and the thermal impedance of the VCSELs in the entire temperature range without having to use pulsed measurements. The two VCSELs exhibit similar internal temperature (displayed in Figure 7a) and thermal impedance (displayed in Figure 7b) throughout the temperature range, as expected because of the identical DBR designs. The difference in detuning is not expected to have an impact on either thermal impedance or internal temperature.

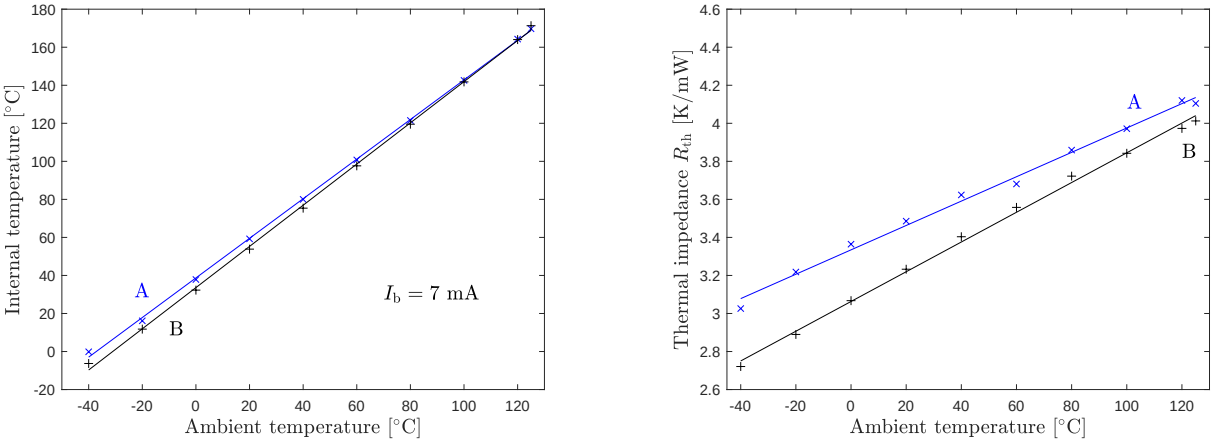

(a) (b)

Figure 7: Internal temperature at 7 mA (a) and thermal impedance (b) as a function of temperature, deduced from spectral and IPV-measurements.

4. DYNAMIC PERFORMANCE CHARACTERISTICS

The dynamic VCSEL behavior, largely dictated by the above threshold carrier-photon interaction, is commonly described by rate equations. The modulation response of the VCSEL can thus be derived from the rate equations and approximated by the following transfer function (with the intrinsic response representing a 2nd order system):[11]

$$H(f) = \text{ const } \times \frac{f_\mathrm{r}^2}{f_\mathrm{r}^2 - f^2 + j(f/2\pi)\gamma} \times \frac{1}{1 + j\,(f/f_\mathrm{p})}, \tag{2}$$

where const is a scaling factor and f_r is the resonance frequency. In the last term, f_p represents the bandwidth limitation caused by the parasitic capacitance of the VCSEL, which in combination with the series resistance forms a low-pass RC-filter. The damping factor γ is proportional to the square of the resonance frequency: $\gamma = K f_\mathrm{r}^2 + \gamma_0$, where γ_0 is the damping offset.[12] The rate at which the resonance frequency increases with bias current (I) is quantified by the D-factor:[12]

$$f_r = D\sqrt{I - I_\mathrm{th}}, \quad D = \frac{1}{2\pi} \cdot \sqrt{\frac{\eta_\mathrm{i}\Gamma v_\mathrm{g}}{qV_\mathrm{a}} \cdot \frac{\partial g/\partial n}{\chi}} \tag{3}$$

where Γ is the optical confinement factor, v_g the group velocity, q the elementary charge, V_a the active region volume, $\partial g/\partial n$ the differential gain, and χ is the transport factor.

To study the dynamics of the VCSELs, we conducted small-signal modulation response (S_{21}) measurements using a 67 GHz vector network analyzer (VNA). The experimental setup is similar to the one used for spectral measurements and described in Section 3, but the VCSEL is biased through the VNA and the lensed fiber outputs to a high-speed photodetector which converts the optical signal to electrical signal and feeds that back into the VNA. Figures 8 and 9 display the measured small-signal modulation response of the VCSELs alongside fits of the transfer function (equation 2). The data is presented throughout the studied temperature range for various bias currents corresponding to typical current densities (20 to 30 $\mathrm{kA/cm^2}$) occurring in the operation of datacom VCSELs.

VCSEL A (Figure 8) exhibits strong peaking at low temperatures due to low resonance frequency, and a more damped response at high temperatures due to higher resonance frequency. Since the resonance frequency is proportional to the square root of current above threshold, quantified by D-factor through equation 3, the resonance frequency is lower in regions of high threshold current at a given bias current. In addition, at low temperatures this effect is augmented because the VCSEL operates at the long wavelength side of the gain peak where differential gain is reduced. Contrarily, the differential gain is higher on the short wavelength side of the gain peak and therefore the response is more damped at high temperatures because of higher resonance frequency, and because of the lower threshold current. VCSEL B (Figure 9), on the other hand, displays a relatively flat response over the entire temperature range due to a better balance of resonance frequency and differential gain over temperature.

To quantify these effects more clearly, we extracted the temperature dependence of the -3 dB bandwidth, the resonance frequency f_r, the modulation response overshoot, the damping rate γ, and the D-factor. As will be shown, variations of differential gain (lower on long wavelength side of gain peak, higher on short wavelength side, decreasing with temperature at all wavelengths) and threshold current with temperature are reflected in the temperature dependence of bandwidth, resonance frequency, and damping rate. The drop in bandwidth and resonance frequency at high temperature is accelerated by the drop in internal quantum efficiency.

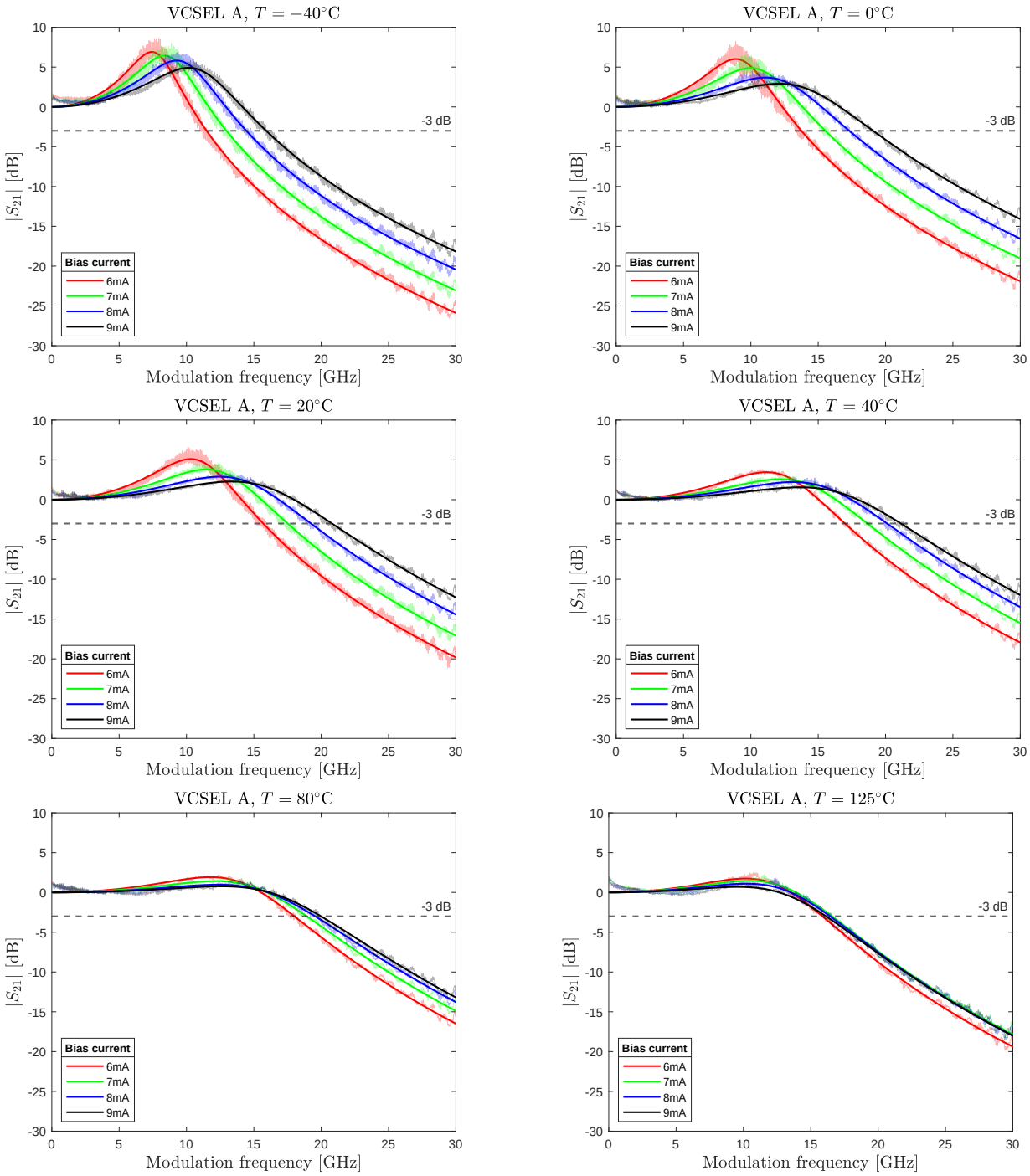

Figure 8: Modulation response of VCSEL A at different ambient temperatures and bias currents. Noisy data represents experimental results, while smooth line is the best fit to Equation 2.

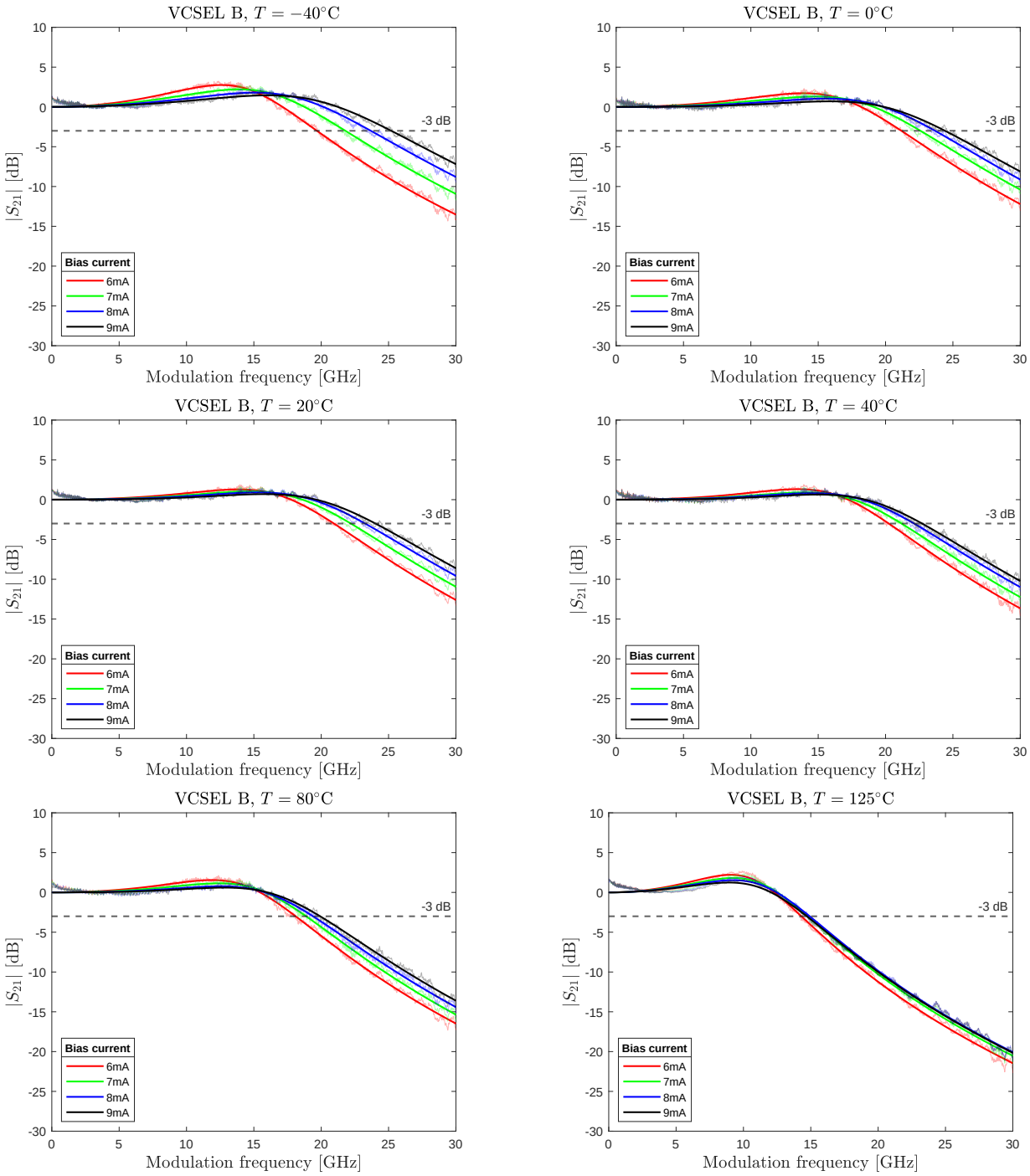

Figure 9: Modulation response of VCSEL B at different ambient temperatures and bias currents. Noisy data represents experimental results, while smooth line is the best fit to Equation 2.

The temperature dependence of the bandwidth (Figure 10) is strongly correlated with detuning, and therefore with the threshold current. Note that while VCSEL A (Figure 10a) exhibits better relative performance at higher temperatures, its low temperature performance is much worse compared VCSEL B (Figure 10b). At 7 mA, design A reaches a maximum bandwidth of 19.2 GHz at 60 °C, while design B reaches 22.6 GHz at −20 °C.

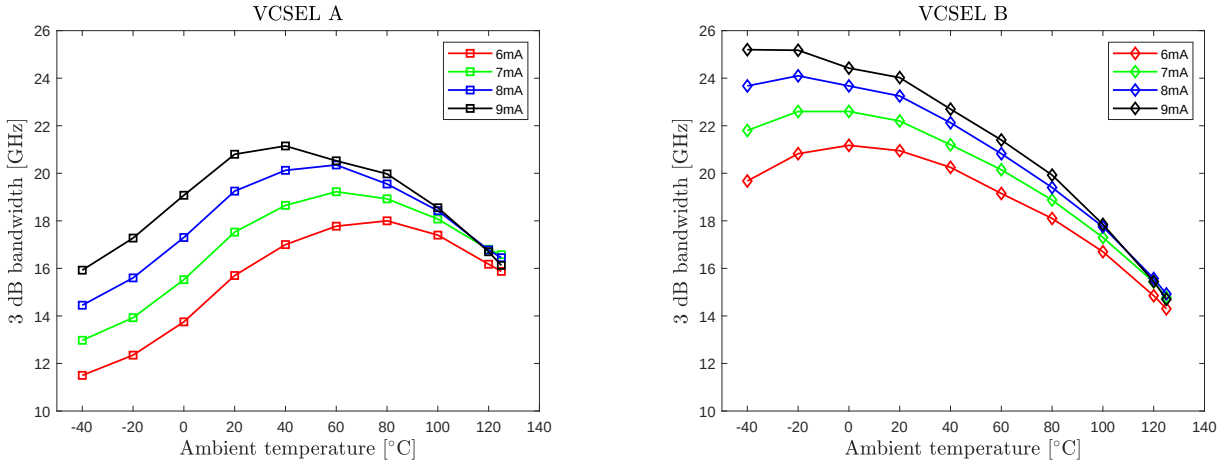

Figure 10: Temperature dependence of -3 dB bandwidth at different bias currents for a) VCSEL A and b) VCSEL B.

Similar behavior can be seen for the temperature dependence of the resonance frequency (Figure 11), which is also strongly correlated with temperature dependence of threshold current. VCSEL A exhibits relatively high threshold current and therefore low resonance frequency at low temperatures, and relatively low threshold current and high resonance frequency at high temperatures (Figure 11a). Opposite behavior can be seen for VCSEL B (Figure 11b). At 7 mA bias, VCSEL A reaches a maximum resonance frequency of 15.9 GHz at 80 °C ($I_{\mathrm{th,min}}$ at 70 °C), while VCSEL B reaches a maximum resonance frequency of 19.2 GHz at 20 °C ($I_{\mathrm{th,min}}$ at 0 °C).

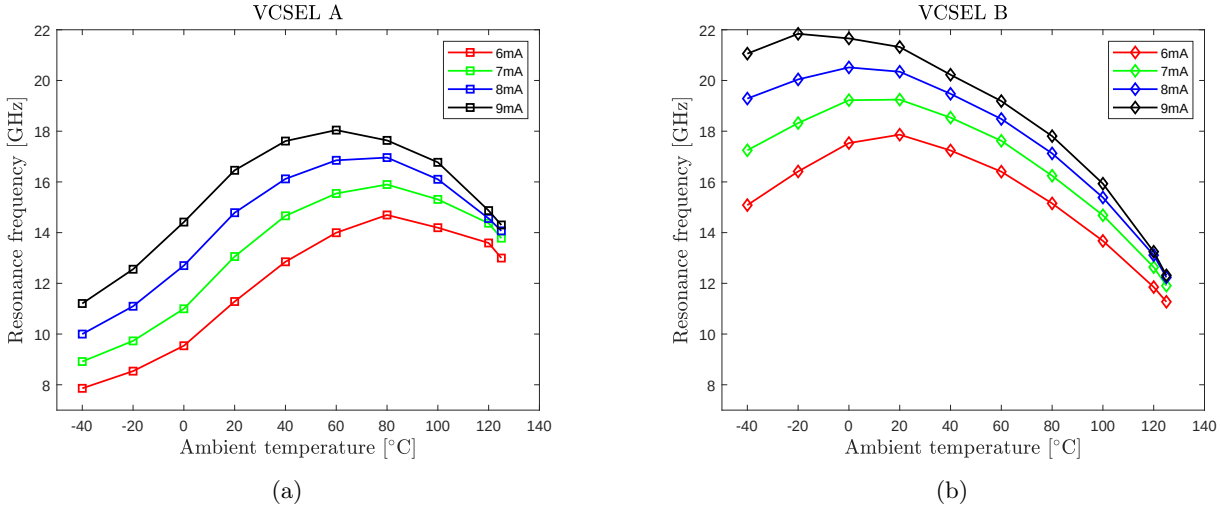

Figure 11: Temperature dependence of resonance frequency at different bias currents for a) VCSEL A and b) VCSEL B.

The flat modulation response of VCSEL B over the entire temperature range is evident from the temperature dependence of overshoot (displayed in Figure 12b). At a bias current of 7 mA, the overshoot is only 2.5 dB or less from −40 °C to 125 °C. VCSEL A (displayed in Figure 12a), on the other hand, exhibits very strong peaking with 6.5 dB overshoot at 7 mA bias at low temperatures. This can cause problems, as strong peaking leads to

significant degradation of signal quality during large signal NRZ or PAM4 modulation, with transient overshoot and ringing causing timing jitter and horizontal eye closure when ringing does not settle within a bit or symbol time slot.[13]

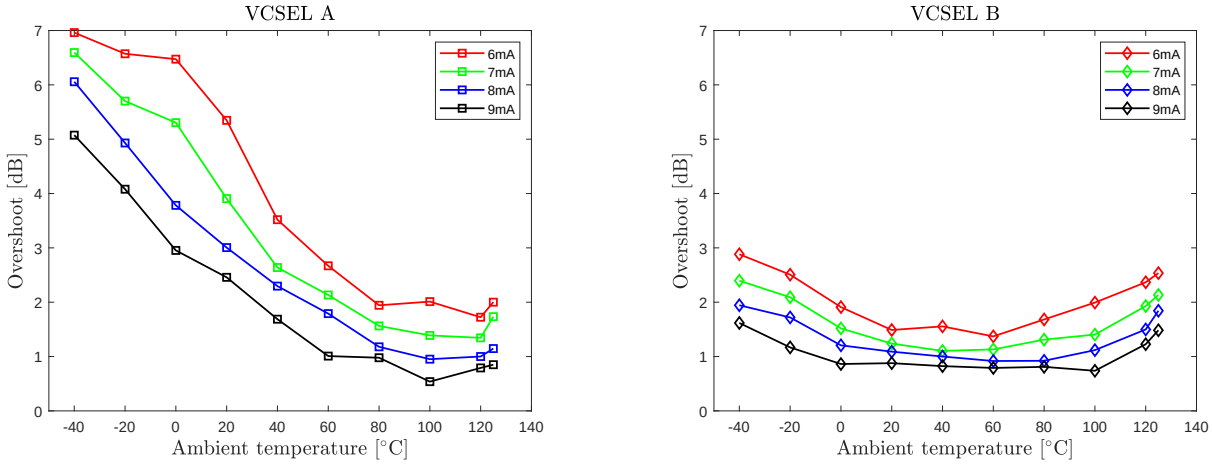

Figure 12: Temperature dependence of overshoot at different bias currents for a) VCSEL A and b) VCSEL B.

The variation of damping rate γ with temperature is presented in Figure 13. The K-factor is not presented here, but was found to be weakly dependent on temperature. Therefore, the variation of damping rate is controlled mainly by the variation of resonance frequency. Thus, γ and f_r have similar temperature dependence, as evident when comparing Figures 11 and 13.

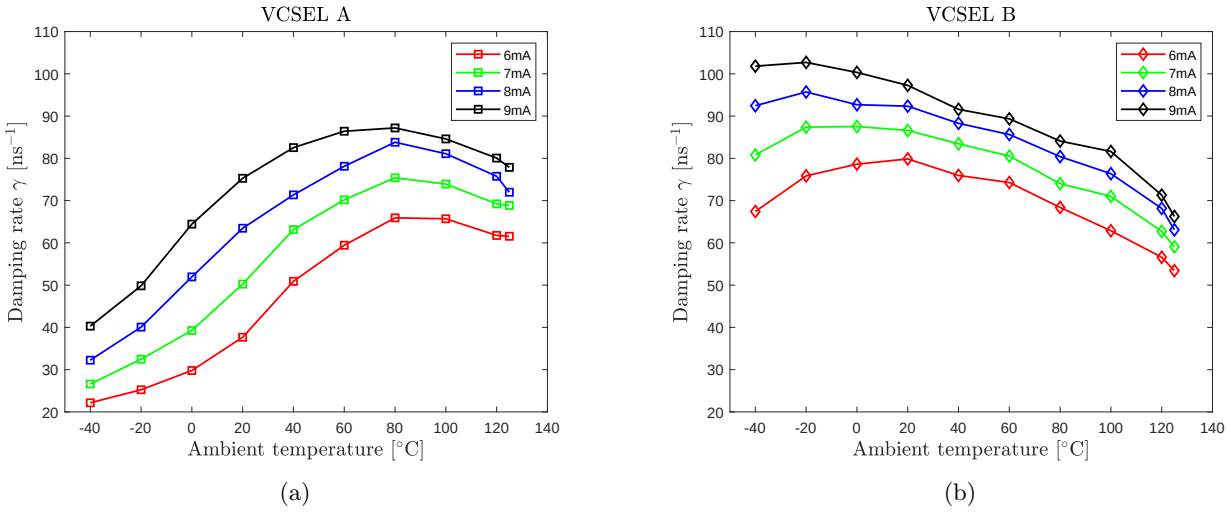

Figure 13: Temperature dependence of damping rate at different bias currents for a) VCSEL A and b) VCSEL B.

The temperature dependence of threshold current, and therefore carrier density and differential gain, is also reflected in the temperature dependence of the D-factor (displayed in Figure 14). VCSEL A exhibits a maximum D-factor of 6.4 GHz/$\sqrt{\text{mA}}$ at 100 °C, while it peaks at 20 °C at 7.8 GHz/$\sqrt{\text{mA}}$ for VCSEL B.

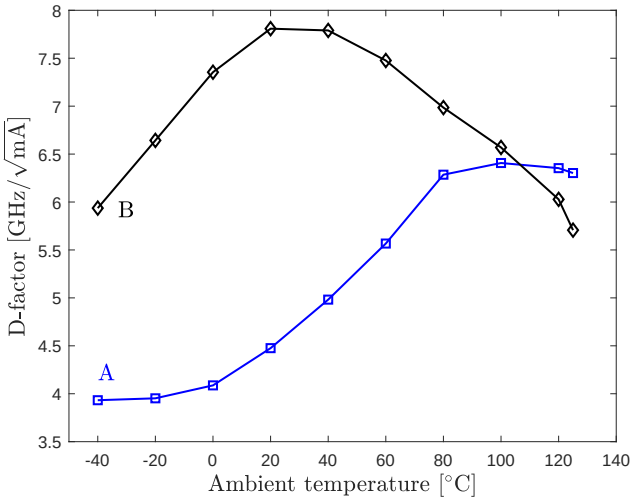

Figure 14: Temperature dependence of the D-factor for VCSEL A and VCSEL B.

5. SUMMARY

We have experimentally studied the impact of detuning on the performance of 25 Gbaud 850 nm VCSELs at temperatures from −40 to 125 °C using two VCSELs with different detuning but otherwise identical. Detuning has a significant effect on the temperature dependence of key performance parameters and is the prime parameter for engineering the VCSEL design for sufficient performance at temperature extremes and robustness against temperature variations. From measurements of static and dynamic characteristics over temperature, we extracted the temperature dependence of multiple performance parameters. While reductions of gain and differential gain with temperature, as well as the reduction of internal quantum efficiency at high temperatures, degrade performance with increasing temperature, the variation of threshold current with temperature, which is strongly impacted by detuning, is clearly reflected in the temperature dependence of several dynamic performance parameters. This is partly because carrier density, and therefore differential gain, depends on threshold current and partly because the difference between bias and threshold currents controls the resonance frequency. Finally, operating at or on the short wavelength side of the gain peak, where differential gain is high, over most of the temperature range, is beneficial for maintaining performance over temperature. We conclude that the detuning used in most present days datacom VCSELs intended for a more limited temperature range, which sets minimum threshold current at around 0 °C, is close to optimum also for the extended temperature range. Increasing detuning to improve performance at very high temperatures results in severe performance degradation at very low temperatures.

ACKNOWLEDGMENTS

The authors would like to thank Stavros Giannakopoulos for assistance with various practical aspects of the measurements. This work was supported by the Swedish Foundation for Strategic Research (SSF) under project HOT-OPTICS, CHI19-0004.

REFERENCES

[1] Tatum, J. A., Graham, L. A., Guenter, J. K., and Khurana, P., "Commercialization of VCSELs," in [*2021 26th Microoptics Conference (MOC)*], 1–2 (2021).
[2] Yole Group, "Market and technology trends: VCSEL 2022," (8 2022).
[3] TRUMPF Photonic Components GmbH, *VCSEL 25 Gbps 850 nm* (1 2022).
[4] II-VI Incorporated, *850nm 25Gb/s Dual Top Contact Multimode VCSEL Array* (2020). Rev. 01.

[5] Kuchta, D., "High speed VCSELs and co-packaging for short reach communication within cloud and high performance computing," in [*2019 24th Microoptics Conference (MOC)*], 298–299 (2019).

[6] Li, H., Wolf, P., Moser, P., Larisch, G., Mutig, A., Lott, J. A., and Bimberg, D. H., "Impact of the quantum well gain-to-cavity etalon wavelength offset on the high temperature performance of high bit rate 980-nm VCSELs," *IEEE Journal of Quantum Electronics* **50**(8), 613–621 (2014).

[7] Petermann, K., [*Laser diode modulation and noise*], Kluwer Academic Publishers, Tokyo (1988).

[8] Nakwaski, W., "Thermal aspects of efficient operation of vertical-cavity surface-emitting lasers," *Optical and Quantum Electronics* **28**, 335–352 (1996).

[9] Westbergh, P., Safaisini, R., Haglund, E., Gustavsson, J. S., Larsson, A., and Joel, A., "High-speed 850-nm VCSELs with 28 GHz modulation bandwidth for short reach communication," in [*Vertical-Cavity Surface-Emitting Lasers XVII*], Choquette, K. D. and Guenter, J. K., eds., **8639**, 86390X, International Society for Optics and Photonics, SPIE (2013).

[10] Daubenschüz, M. and Michalzik, R., "Parameter extraction from temperature-dependent light-current-voltage data of vertical-cavity surface-emitting lasers," in [*Semiconductor Lasers and Laser Dynamics VII*], Panajotov, K., Sciamanna, M., Valle, A., and Michalzik, R., eds., **9892**, 98920R, International Society for Optics and Photonics, SPIE (2016).

[11] Kjebon, O., Schatz, R., Lourdudoss, S., Nilsson, S., and Stalnacke, B., "Modulation response measurements and evaluation of MQW InGaAsP lasers of various designs," in [*High-Speed Semiconductor Laser Sources*], Morton, P. A. and Crawford, D. L., eds., **2684**, 138 – 152, International Society for Optics and Photonics, SPIE (1996).

[12] Coldren, L. and Corzine, S., [*Diode Lasers and Photonic Integrated Circuits*], Wiley, New York (1995).

[13] Lengyel, T., Szczerba, K., Haglund, E. P., Westbergh, P., Karlsson, M., Larsson, A., and Andrekson, P. A., "Impact of damping on 50 Gbps 4-PAM modulation of 25G class VCSELs," *Journal of Lightwave Technology* **35**(19), 4203–4209 (2017).